

ADVANCED MATERIALS

SILICON NANOMEMBRANES

The ability of silicon to dissolve in physiological environments allows its use as the basis of a high-performance inorganic integrated circuit technology for active, bioresorbable implant devices. N. R. Aluru, J. A. Rogers, and co-workers perform systematic experimental and theoretical studies of hydrolysis of silicon nanomembranes at near neutral pH, as described on page 1857. This image shows a molecular-dynamics rendering of nucleophilic attack of a silicon surface immersed in water and the resulting formation of molecules of silicic acid.

Mechanisms for Hydrolysis of Silicon Nanomembranes as Used in Bioresorbable Electronics

Lan Yin, Amir Barati Farimani, Kyoungmin Min, Nandigana Vishal, Jasper Lam, Yoon Kyeong Lee, Narayana R. Aluru,* and John A. Rogers*

Long-lasting, reliable operation is a hallmark of traditional integrated circuit technologies. Recent work suggests that electronics whose distinguishing characteristic is an ability to completely or partially disappear in a well-defined manner after a prescribed functional lifetime can yield unique and alternative types of devices.^[1] Attractive applications for this kind of “transient” electronics range from biomedical implants that resorb, thereby obviating the need for surgical retrieval, to environmental sensors that dissolve, thereby eliminating solid electronic waste.^[1–4] Degradable organic electronic materials can be contemplated for use in such systems.^[5–7] The recent discovery that silicon nanomembranes (Si NMs) undergo hydrolysis in biofluids and ground/sea water provides an opportunity to adapt well-established, high performance inorganic integrated circuit technology for transient electronics.^[1] In particular, Si NMs can be combined with water soluble, biocompatible electrodes, and interconnect metals (e.g., magnesium (Mg), zinc (Zn), tungsten (W) or molybdenum (Mo)),^[8] interlayer, and gate dielectrics (e.g., silicon dioxide (SiO₂), magnesium oxide (MgO) or silicon nitride (Si₃N₄)),^[1,9] and biodegradable polymer substrates (e.g., polycaprolactone, poly(lactic-co-glycolic acid)),^[3,10] to yield diverse classes of transient devices. The use of inorganic materials that are not only degradable but also fully dissolvable into biocompatible ions in physiological solutions and of organic biodegradable polymers that can be broken down into digestible small molecules, endows transient electronics with bioresorbable and eco-resorbable characteristics. Demonstrated applications

include thermal therapy systems to mitigate surgical site infections,^[1] radio-frequency energy harvesters and oscillators,^[11] primary battery systems,^[12] and many others.^[1,10,13]

Silicon is often considered to have excellent chemical stability, due partly to its native oxide.^[14] At nanoscale thicknesses (i.e., in the form of nanomembranes), however, even slow rates of reaction and material degradation can be important. For example, silicon can undergo hydrolysis at rates that completely consume Si NMs in only a few days or weeks,^[1] with similar behavior in silicon nanowires.^[15] The reaction product, silicic acid Si(OH)₄, is a naturally occurring component in biofluids (typical concentrations in serum range from 14×10^{-6} to 39×10^{-6} M)^[16] and is found in ground water (typically from 0.4×10^{-6} to 180×10^{-6} M)^[17] and sea water (up to 100×10^{-6} M).^[17] Results from implantation of Si NMs in live animal models (mice) suggest good biocompatibility at mass levels that are capable of supporting practical levels of electronic function.^[2,18] When taken together with silicon's essential role in conventional integrated circuit technology, these observations make Si NMs an ideal choice for the semiconductor in bioresorbable and environmentally degradable electronics. A fundamental understanding of the kinetics of hydrolysis of Si NMs is, therefore, important. Consistent with previously reported results on porous silicon structures for drug release,^[19,20] on silicon nanowires for biosensors,^[15] and on bulk wafers for microelectromechanical systems,^[21,22] hydrolysis can depend on many factors, including temperature, pH and doping level.^[1,2,18,21,22] Rates of dissolution of Si NMs with light doping levels (10^{-17} cm⁻³, p-type) range from a few nanometers to 100 nm per day in biological solutions at body temperature (37 °C).^[1,2,18] Although hydroxyl ions (OH⁻) are generally thought to be the main species responsible for hydrolysis, experimental data show that in physiological solutions with mild pH, Si NMs can be consumed at up to 100 nm per day in bovine serum (\approx protein 40 g L⁻¹, \approx 0.12 M sodium chlorides, pH 7.4 at 37 °C), corresponding to a rate that is 20 times higher than that in phosphate buffered saline solution at comparable pH (\approx 0.14 M chlorides and 0.01 M phosphates, pH 7.4 at 37 °C). The typical composition of various physiological solutions is given in Table S1 (Supporting Information). As another example, a recent, unspecified change in the formulation of a commercial phosphate buffer solution (1 M, pH 7.4, Sigma–Aldrich) led to a factor of 10 change in the dissolution rates.^[2] Such results suggest that ions and/or proteins can strongly affect the rate of the hydrolysis reaction. Combined experimental and theoretical studies presented here examine the underlying aspects as a function of concentration of anions (i.e., chlorides (Cl⁻) and phosphates (HPO₄²⁻)) that are found in biological systems.^[23,24] An empirical model describes

Dr. L. Yin, Prof. J. A. Rogers
Department of Materials Science and Engineering
Beckman Institute for Advanced Science and Technology
Frederick Seitz Materials Research Laboratory
University of Illinois at Urbana-Champaign
Urbana, IL 61801, USA
E-mail: jrogers@illinois.edu



A. B. Farimani, K. Min, N. Vishal, Prof. N. R. Aluru
Department of Mechanical Science and Engineering
Beckman Institute for Advanced Science and Technology
University of Illinois at Urbana-Champaign
Urbana, IL 61801, USA
E-mail: aluru@illinois.edu

J. Lam
College of Liberal Arts and Sciences
University of Illinois at Urbana-Champaign
Urbana, IL 61801, USA

Y. K. Lee
Department of Chemistry
Frederick Seitz Materials Research Laboratory
University of Illinois at Urbana-Champaign
Urbana, IL 61801, USA

DOI: 10.1002/adma.201404579

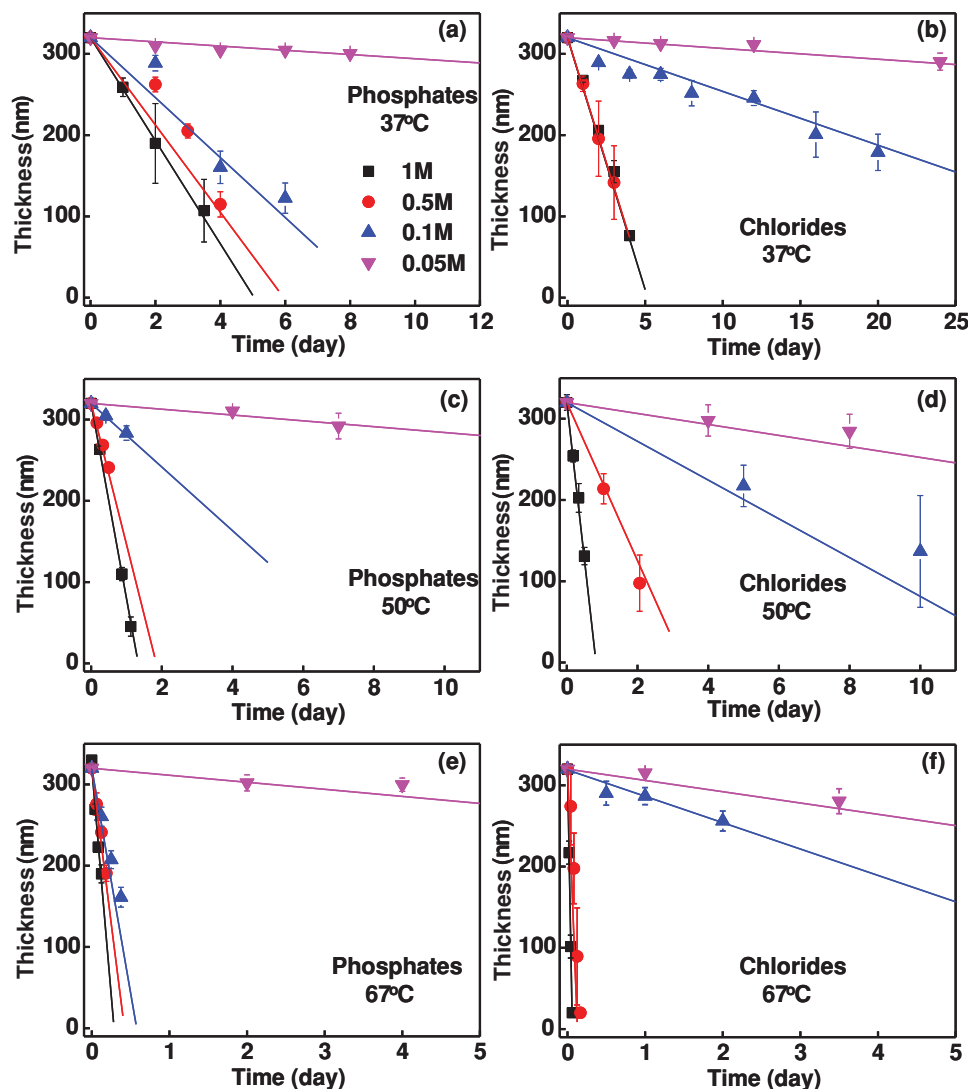


Figure 1. Change in thicknesses of Si NMs as a function of time of immersion in aqueous solutions of potassium phosphates and potassium chlorides with different concentrations, evaluated at different temperatures: a,b) 37 °C; c,d) 50 °C; e,f) 67 °C. The lines correspond to fits to empirical models.

the dependence of the dissolution rates on key factors, and atomic level simulations provide insights into the underlying chemistry.

Dissolution of Si NMs (slightly p-doped 10^{-17} cm^{-3} , 100 orientation, 320 nm thickness, derived from the top silicon layer of a silicon on insulator (SOI) wafer) as a function of ion concentration (chlorides and phosphates, 0.05–1 M) and temperature (37–67 °C) at a fixed pH of 7.5 illustrate the key dependencies. As shown in **Figure 1**, the change in thickness as a function of time indicates linear reaction kinetics for all cases. The rates span a range of nearly four orders of magnitude, as summarized in **Figure 2**. The range of the *x*-axes and the number of data points and frequency of data collection for the results of **Figure 1** depend on the rate of change of the Si NM thickness. The dissolution rates in phosphate solutions of 0.05 M and chloride solutions of 0.05 and 0.10 M are relatively slow, with data collection at longer intervals compared to those for solutions with higher concentrations, until an obvious

decrease in thickness can be observed for extraction of the dissolution rates. The anions likely play a prominent role in the reactions, since silicon is known to be susceptible to nucleophilic attack.^[14] For similar concentrations, chloride and phosphate solutions yield significantly different rates, especially at 0.1 M concentration and at 67 °C. In all instances, the rates increase with temperature, consistent with Arrhenius behavior as will be discussed subsequently and in the Supporting Information (**Figure S1**, Supporting Information).

Extensions of empirical models previously used to describe silicon etching in concentrated KOH solutions (10–60 wt%, for pH between 13 and 14) by Seidel et al.^[21] can capture the experimentally observed trends. As will be described by density functional theory (DFT) simulations subsequently, chlorides and phosphates can play important roles in the reactions. The activation energy and dissolution rate are therefore expected to depend on the concentration of these species. We postulate that the rates can be written as:

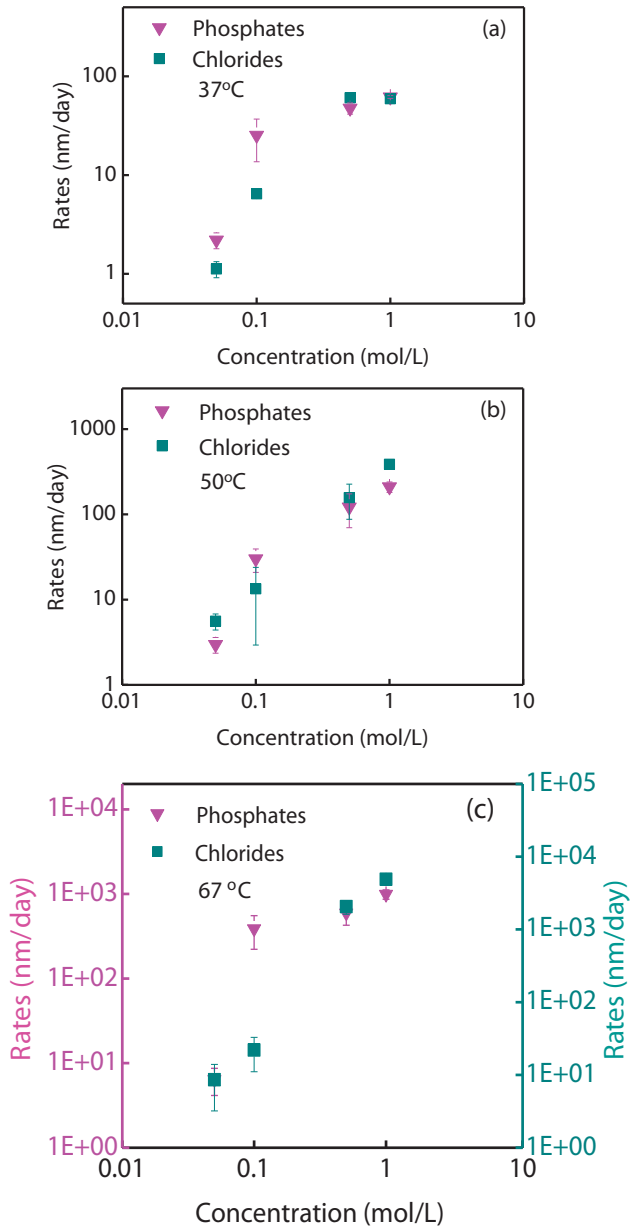


Figure 2. Summary of rates of dissolution for Si NMs in various solutions at different temperatures: a) 37 °C; b) 50 °C; c) 67 °C.

$$r^{\text{model}} = k_0 \exp\left(-\frac{E_a(\text{PO}_4^{3-})}{k_B T}\right) [\text{H}_2\text{O}]^4 [\text{OH}^-]^{0.25} [\text{PO}_4^{3-}]^{0.25} \quad (1)$$

$$r^{\text{model}} = k_0 \exp\left(-\frac{E_a(\text{Cl}^-)}{k_B T}\right) [\text{H}_2\text{O}]^4 [\text{OH}^-]^{0.25} [\text{Cl}^-]^{0.25} \quad (2)$$

$$k_0 = 2480 \mu\text{m hr}^{-1} (\text{mol/L})^{-4.5} \quad (3)$$

Here, the pre-exponential factor k_0 is a constant, with a value determined from previous studies of silicon etching at high pH (10–60 wt% KOH solutions, for pH between 13 and 14).^[21] The

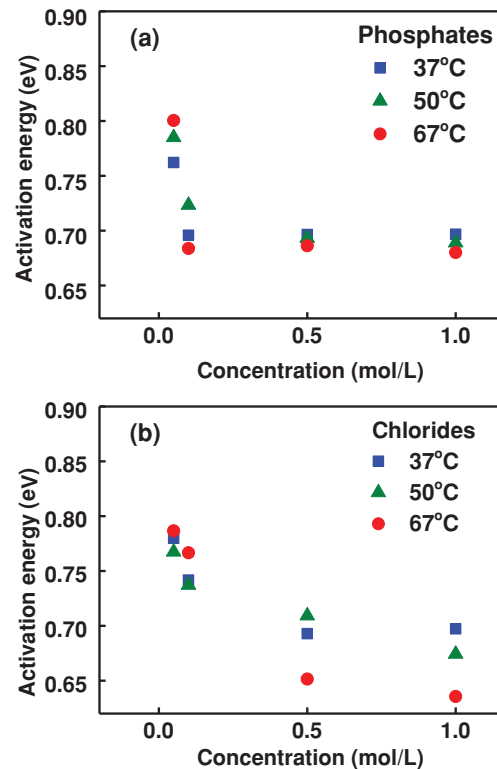


Figure 3. Activation energies determined from fitting averaged measured dissolution rates to empirical models as a function of concentration: a) phosphates; b) chlorides.

concentration of water is approximately constant (55.6 M, to within $\approx 10\%$) for the range of temperatures and concentrations examined here. The pH (7.5 for present results) determines the concentration of OH^- . The reaction orders for the phosphate and chloride ions are taken to be $\frac{1}{4}$ (same as that for OH^-), based on an assumption, discussed in detail subsequently, that their reaction configurations are similar to those for OH^- . The activation energies, E_a , follow from fitting to experimental observations (averaged dissolution rates in each condition). The results indicate some systematic dependence of E_a on concentration (0.64–0.84 eV), and slight changes with temperature (Figure 3). The former is consistent with results from studies of silicon etching,^[21] the latter is consistent with Arrhenius scaling and activation energies fitted using Equation 1 and 2 (Figure S1, Supporting Information).

Dissolution of silicon in highly concentrated KOH solutions (10–60 wt%, pH 13–14) is believed to proceed through nucleophilic attack of silicon surface bonds by OH^- ,^[14] which weakens the interior bonds of surface silicon atoms (backbonds) and increases their susceptibility to further OH^- attack. As a result, silicon dissolves in a layer by layer fashion, yielding $\text{Si}(\text{OH})_4$ in the surrounding solution, without significant formation of oxides on the surface.^[21] Physiological conditions involve pH values that are near neutral, where the concentration of OH^- (pH ≈ 7.5 , $10^{-6.5}$ M) is much lower than that of other anions such as chlorides and phosphates (typically ≈ 0.001 – 0.2 M).^[23,24] Such species can act as nucleophiles, to promote dissolution. In these conditions, silicon oxide is likely to be unstable

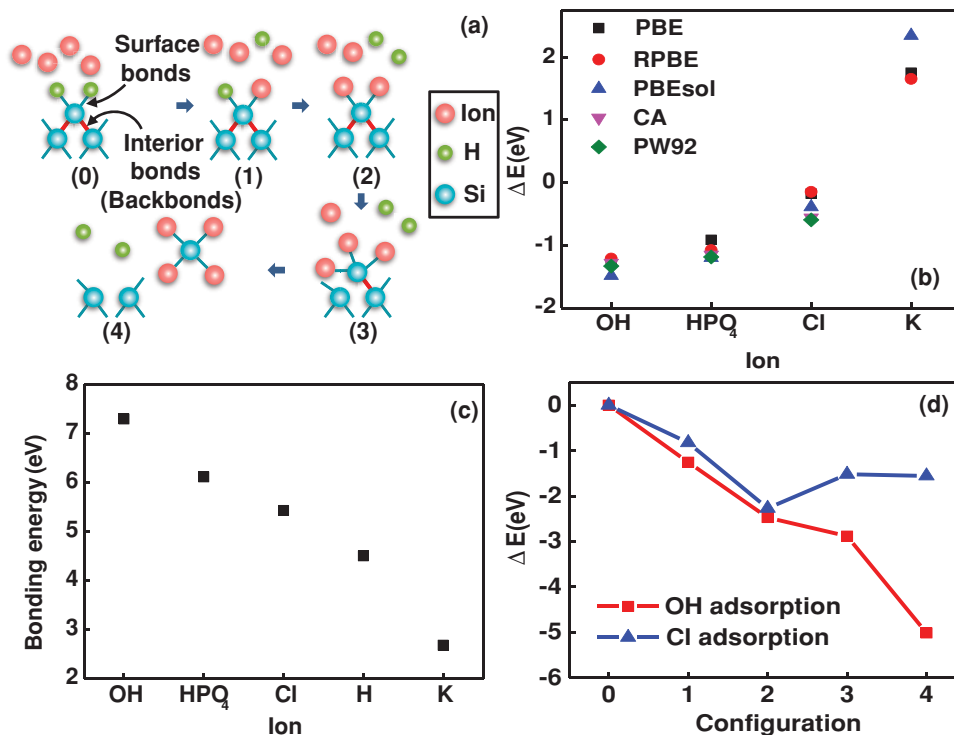


Figure 4. DFT modeling of the silicon dissolution process: a) atomic configurations for each ion adsorption event; b) comparison of the change in energy computed using different XC functionals for different ions. Bonding preference: OH > HPO₄ > Cl, the K–Si bond is not preferred over K–H; c) strength of ion–Si bonds. d) Change in energy as a function of number of ions (OH or Cl) bonded to Si.

and/or present at low coverage, consistent with the simple, linear kinetics of Figure 1 and previous reports.^[2,18]

Simulations based on density functional theory lend some support for the hypothesized role of anions in weakening the silicon interior bonds. A schematic view of the adsorption process for ions (OH[−], HPO₄^{2−}, Cl[−], K⁺) on the silicon surface is shown in Figure 4a. HPO₄^{2−} is chosen to represent the effects of phosphates, since it accounts for ≈80 molar percent of the phosphate buffer solutions at pH 7.5. Computing the change in energy between configuration (0) and (1) for each ion individually yields information relevant to reactivity and bond preferences. Configuration details appear in Figure S2 (supporting information). Structural relaxation following placement of the ion (or H⁺) with a distance of ≈3 Å from the silicon surface defines the equilibrium bond-length. The computed bond lengths for Si–O, Si–H, Si–K, and Si–Cl show reasonable agreement with those reported previously (Table S2, supporting information).^[25–28] The total change in energy ($\Delta E_{\text{ion}} = E_{\text{Bonded}} - E_{\text{Nonbonded}}$, where E_{Bonded} and $E_{\text{Nonbonded}}$ are the energies of the system when an ion is bonded and nonbonded, respectively) for each ion is shown in Figure 4b. The results from different exchange–correlation (XC) functional forms are compared for further verification of DFT calculations. The Perdew–Burke–Ernzerhof (PBE) functional is used for the rest of the calculations. The total change in energy agrees well using both local density approximation (LDA) and generalized gradient approximation (GGA) functionals. The findings suggest that the bonding preference is Si–OH > Si–HPO₄ > Si–Cl, with Si–H preferred over Si–K. For experimental conditions reported here, the high concentration of Cl[−] and HPO₄^{2−}

compared to that of OH[−] suggests that three different ions (OH[−], HPO₄^{2−}, and Cl[−]) can form bonds with the silicon. The computed bonding energy (E_{Bonding}) for each adsorption case can further establish the bonding preferences. Here, E_{Bonding} is $E_{\text{Si+Ion}} - (E_{\text{Si}} + E_{\text{Ion}})$, where $E_{\text{Si+Ion}}$ is the total energy of the silicon with bonded ions, and E_{Si} and E_{Ion} are the energies of the isolated silicon structure and each ion, respectively. Figure 4c summarizes the values of E_{Bonding} ; the results agree with previous reports^[29,30] and are consistent with those in Figure 4b, where OH[−] > HPO₄^{2−} > Cl[−] > H⁺ > K⁺.

Nucleophilic ions bonded to the silicon surface can weaken the interior bonds of silicon surface atoms. Computed lengths of the interior bonds following adsorption of OH[−], Cl[−], and HPO₄^{2−} appear in Table 1. In each case, bonding elongates the

Table 1. Length of interior bonds of surface silicon atoms (backbonds) following adsorption of different ions. The designations left and right correspond to the interior bonds illustrated in Figure 4a. For HPO₄ adsorption, configurations 2 to 4 are not considered because the structure becomes energetically unstable during minimization.

Configuration	Bond length [Å]		
	Si–Si back bonds (left, right)		
	OH adsorption	Cl adsorption	HPO ₄ adsorption
0	2.350, 2.350	2.351, 2.351	2.350, 2.350
1	2.357, 2.359	2.355, 2.356	2.356, 2.356
2	2.365, 2.369	2.385, 2.376	–
3	2.368, 3.340	2.409, 3.869	–
4	3.934, 3.826	4.345, 4.426	–

silicon interior bonds, implying a weakening in their strength. Although the increased length is relatively small ($\approx 10^{-2}$ Å), this behavior occurs consistently for OH^- , Cl^- , and HPO_4^{2-} . Due to the decreased strength, the interior bond is susceptible to breakage when a third ion is introduced in the DFT system. The DFT findings therefore qualitatively support the hypothesized mechanism that Cl^- and HPO_4^{2-} can interact with the silicon surface in a manner similar to OH^- . In particular, these ions can bond with the silicon surface to weaken the interior bonds of silicon surface atoms, and assist in silicon dissolution, as observed in experiments (Figure 1 and 2). A reasonable assumption, explored through molecular dynamics (MD) simulations described next, is that such effects increase with concentration of Cl^- and HPO_4^{2-} . The activation energy of the reaction should depend on the extent of weakening of the interior bonds,^[21] which provides an explanation for the observed dependence of activation energy on concentration (Figure 3). We note that the DFT results on relative bond strengths do not translate directly to dissolution rates, simply because these rates can depend on other factors (e.g., concentration, etc).

The reaction product from interaction of silicon with OH^- ^[31] can be examined by comparing the changes in energy associated with the addition of ions (up to 4 ions, OH^- , and Cl^-) to the silicon surface (Figure 4d). Increasing the number of adsorbed OH^- progressively decreases the energy, which suggests that $\text{Si}(\text{OH})_4$ is energetically more stable than SiCl_4 . On the other hand, Cl^- adsorption is energetically more favorable with the silicon surface (configuration 1 and 2 in Figure 4a) compared with the silicon interior bonds (configuration 3 and 4 in Figure 4a). In other words, $\text{Si}(\text{Cl})_4$ is energetically stable, but cannot be naturally formed in a sequential manner after the surface adsorption of two Cl^- species. $\text{Si}(\text{OH})_4$ is therefore believed to be the most stable final product.

Overall, DFT results suggest that OH^- plays a critical role in dissolution by consequence of a reaction potential that is stronger compared to those of other ions. Nucleophilic anions such as Cl^- and HPO_4^{2-} at different concentrations can accelerate the reaction to varying extents by reacting with surface silicon atoms in a way that weakens the interior bonds. These conclusions are in qualitative agreement with experimental observations, e.g., i) Cl^- concentrations higher than 0.05 M are needed in solutions with $10^{-6.5}$ M OH^- (pH 7.5) to accelerate the silicon dissolution rates to any significant degree; ii) solutions with 10^{-2} and 10^{-4} M OH^- (pH 12 and pH 14) have rates (33 μm and 18.5 nm per day, respectively) higher than that of $10^{-6.5}$ M OH^- (pH 7.5) solutions with 10^{-1} M of Cl^- (6.5 nm per day).

MD simulations can describe the dynamic processes of dissolution. Although active reaction potentials containing Cl^- or HPO_4^{2-} are unavailable, ReaxFF potentials with OH^- provide insights into roles of Cl^- or HPO_4^{2-} , justified by the previously described DFT findings that suggest similar behavior for the nucleophiles (OH^- , Cl^- , and HPO_4^{2-}). MD results show that silicon atoms dissociate and dissolve in water (Figure 5a), starting with the first silicon atom at 6.5 ns (Here, dissociation occurs when the maximum distance of a silicon atom from its nearest neighbors is >3.0 Å; the Si–Si bond length is 2.3 Å). Additional silicon atoms dissociate with an approximately linear kinetics, until $t = 38$ ns (Figure 5a), when dissociation dramatically slows, likely due to the saturation of dissolution products

in the surrounding liquid. A parallel simulation that involves immersing the silicon structure that exists at $t = 78$ ns into fresh water (i.e., dissolution products removed, to leave only water molecules surrounding the structure; “refreshed water” case in Figure 5a), shows renewed silicon dissociation, thereby providing some confirmation that the presence of dissolution products can slow the forward reaction. Although re-adsorption of silicon can occur after reaching the saturation point, such events are not observed within the run time of the simulations. By extending the simulation times, re-adsorption events might be observable. Any such events would appear in Figure 5a as a fluctuation in the number of dissolved Si atoms.

The formation of various species as intermediates to $\text{Si}(\text{OH})_4$ also appear, as shown in Figure 5b, and the cations $\text{Si}(\text{OH})_2^{2+}$ and $\text{Si}(\text{OH})_3^+$ occur frequently. Initially, a single OH^- attacks the Si surface but does not initiate a dissociation process. Figure 5b accounts for the species that appear in the solution. The results indicate that the minimum number of OH^- needed for dissociation of Si is two. Some species interconvert, such as $\text{Si}(\text{OH})_2^{2+}$ to $\text{Si}(\text{OH})_3^+$. A molecule of $\text{Si}(\text{OH})_4$ forms at $t = 87$ ns. Snapshots of detachment of Si atoms from the Si surface and formation of $\text{Si}(\text{OH})_3^+$ are given in Figure 5c. The left image in Figure 5c depicts the initial configuration of a silicon atom (enlarged) that subsequently detaches from the surface and three reacting OH^- groups (the oxygen is shown in blue). Initially, at $t = 6.38$ ns, two OH^- groups attack the silicon atom and form bonds (Figure 5c, middle). At $t = 9.11$ ns, another OH^- group attacks the same silicon atom and triggers its complete dissociation (Figure 5c, right). Consequently, $\text{Si}(\text{OH})_3^+$ is formed and drifts away in the solution.

Studies using solutions at acidic (pH 4.2) and basic (pH 9.2) conditions formed by addition of H^+ and OH^- , respectively, to neutral (pH 7.0) solutions yield information on the effects of nucleophile concentration (i.e., OH^- , and indirectly Cl^- or HPO_4^{2-}). As in Figure 5d, the rates of silicon dissolution for both pH 4.2 and 7.0 are lower than that for pH 9.2. Due to the low concentration of OH^- in the pH 4.2 and 7.0 solutions, short timescale MD simulations do not provide quantitative insights into Si dissolution rates. The rate of silicon oxide formation is also slower for pH 9.2 compared to that for pH 4.2 and 7.0, indicating that free hydroxyl groups play a significant role in preventing surface oxidation and accelerating silicon dissociation (Figure 5e). The first dissociation of Si at pH 4.2 occurs 2 ns earlier than at pH 7.0. This ordering can be attributed to thermal noise and the stochastic nature of processes involved in the reaction dynamics. At 10 ns, the same number of dissociated Si appears for pH 7.0 and 4.2. This result suggests similar trends for dissolution in both solutions. Based on our observations, the number of OH^- must be higher than that of pH 7.0 (neutral) or 4.2 (acidic) to make significant/meaningful changes in the dissolution process. SiO_2 formation in Figure 5e follows similar behavior. The total number of formed SiO_2 becomes equal for pH 7.0 and 4.2 at $t = 10$ ns. The total number of formed SiO_2 is also the same for pH 7.0 and 4.2 at $t = 10$ ns. We speculate that nucleophiles like Cl^- or HPO_4^{2-} could behave similarly, thereby accelerating silicon dissolution and hindering silicon oxide formation, with effects that increase with concentration as in experiments. Such trends appear in the previous reports of increased rates of dissolution of silicon oxide in high

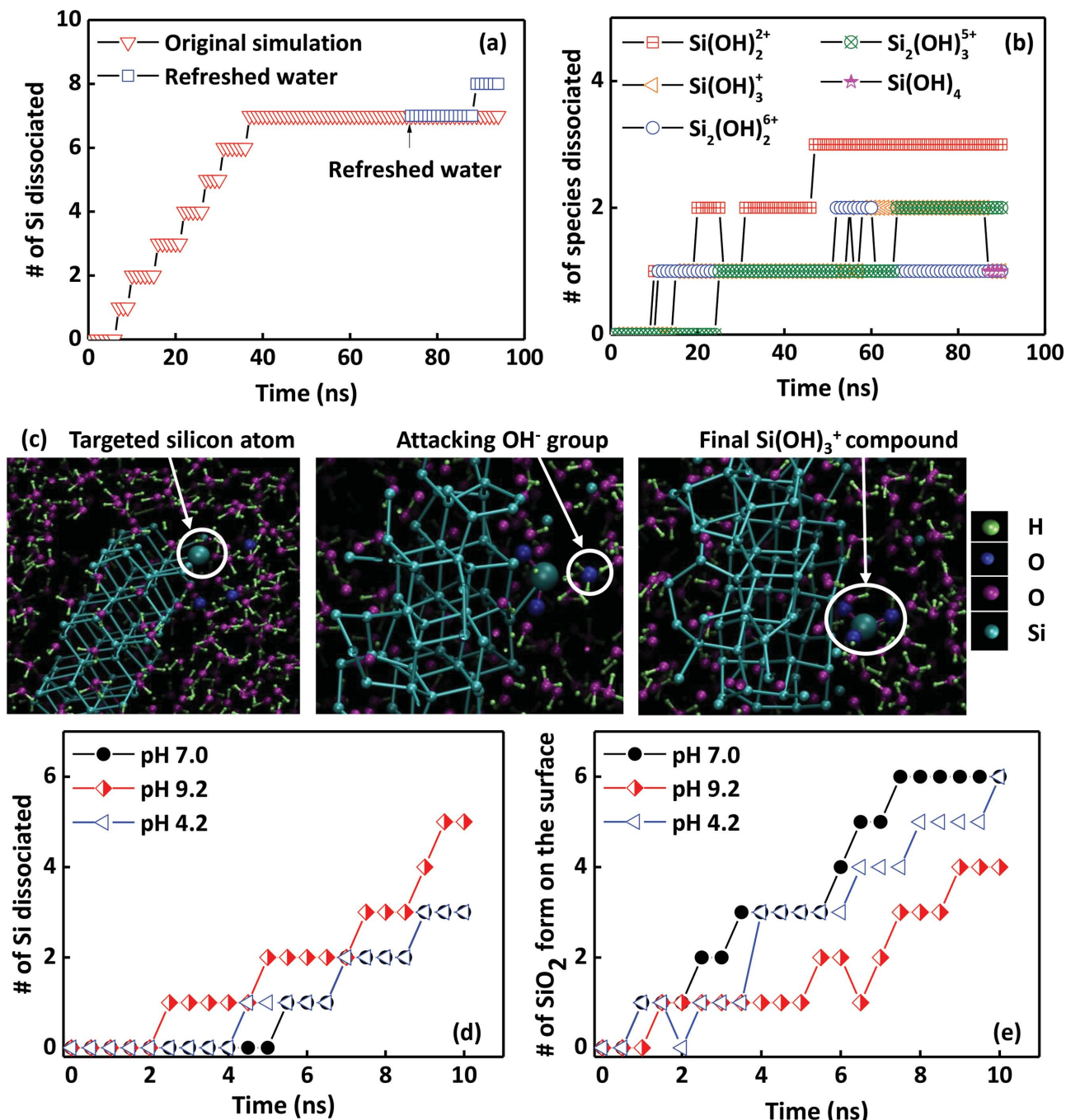


Figure 5. MD modeling of the silicon dissolution process: a,b) Dissolution of silicon in water; c) MD images of silicon dissolution: (Left) Snapshot of the initiation of silicon dissociation (the targeted silicon atom that dissociates in this example appears enlarged and the three attacking water molecules are shown in blue, both for purposes of illustration). (Middle) Bonding of two OH^- groups to the targeted silicon atom, with another approaching OH^- shown in background. (Right) Bonding of the third OH^- group to the targeted silicon atom and complete dissociation of Si through formation of $\text{Si}(\text{OH})_3^+$; d) time-dependent dissolution of silicon at different pH; e) time-dependent oxidation process of silicon at different pH.

concentration phosphate buffer solution (0.01–0.25 M).^[32] These findings also suggest minimal presence of oxide at these experimental conditions (pH > 7), likely due to multiple cycles of formation and immediate dissolution. The dissolution of silicon oxide and direct nucleophilic attack of silicon are therefore both believed to be important.

Moreover, averaging (for the entire simulation time) the density of OH^- and H^+ ions near the surface of Si yields results that indicate that the OH^- ions reside closer to the silicon surface than the H^+ . This observation suggests an affinity of OH^- by physisorption to the silicon surface (Figure S3, Supporting Information), which could

further prevent oxidation of the surface and accelerate silicon dissolution.

The findings reported here illustrate that the kinetics of dissolution of Si NMs depend on anion concentration and temperature. DFT and MD simulations both suggest that chlorides and phosphates interact with the silicon surface in a way that can promote nucleophilic attack by weakening the interior bonds of silicon surface atoms and suppressing surface silicon oxide formation. The resulting expected dependence of the dissolution rate on ion concentration aligns with previously reported data obtained using different aqueous solutions,^[2,18] in which the rates are as follows: i) pH 7.4 at room temperature, spring water (≈ 0.5 nm per day) < phosphate buffered saline (≈ 2.5 nm per day) < bovine serum (≈ 35 nm per day); ii) pH 7.8 at room temperature, tap water (≈ 1 nm per day) < sea water (≈ 4 nm per day).^[2,18] Deionized water gives very small silicon dissolution rates (< 0.1 nm per day) at room temperature due to the absence of ions. Silicon dissolution rates are 30 nm per day in breast cancer cell culture media (\approx pH 7.4, Leibovitz's L-15 medium with 10% fetal bovine serum and 1% penicillin-streptomycin), which are roughly one third of those in bovine serum (100 nm per day) at 37 °C,^[2] possibly due to the absence of bicarbonate and the presence of different proteins. Hanks' solution (pH 7.8), which has a slightly higher concentration of ions than phosphate buffered saline (pH 7.4, ≈ 0.14 M NaCl and 0.001 M phosphates), shows a 12 times higher dissolution rate (60 nm per day vs 5 nm per day at 37 °C) possibly due to the increased pH level and the presence of bicarbonates (0.004 M). The data in the current experiments (37 °C) show that rates increase with concentrations from 0.05 to 1 M (pH 7.5) by a factor of 30 and 60 for phosphates and chlorides, respectively. Such change is consistent with the previously reported factor of ≈ 30 (1 M/0.05 M, pH 7.4) obtained using commercially purchased phosphate buffer solutions.^[2] Additional experimental results demonstrate that the presence of even a few nanometers of surface oxide delays the silicon dissolution (Figure S4, Supporting Information), just as the presence of a separately deposited layer of aluminum oxide can extend the lifetimes of silicon nanowires.^[15] Further studies of silicon dissolution on solution flow rates, lateral size scales, proteins, living cells, and tissues, and various strategies for controlling the lifetime represent next steps. A combination of experimental and computational tools provides insights into the chemistry, highlights fundamental effects, and defines topics for further study, all of foundational relevance to silicon-based water soluble electronics.

Experimental Section

Fabrication of Si NMs and Measurement of their Dissolution: Silicon on insulator (SOI) wafers served as the source of the Si NMs (slightly p-doped 10^{-17} cm⁻³, 100 direction, 320 nm thickness). Photolithography (AZ5214) and reactive ion etching (RIE) with SF₆ gas defined Si NMs with square geometries (10 × 10 μm) in array formats. Phosphate buffer solutions with different concentrations at pH 7.5 were prepared using potassium phosphate monobasic and dibasic (molar ratio 19.8/80.2, Sigma-Aldrich Corporation, St. Louis, MO, USA). Buffered potassium chloride solutions were prepared in 0.001 M phosphate buffer solutions with different amounts of potassium chloride to maintain a constant pH. Immersion of the Si NMs (on the SOI platforms) in buffered oxide

etchant (BOE) (6:1) eliminated the native oxide just prior to insertion into constantly stirred solutions, with the target temperature maintained using a hot plate. The thickness was determined by profilometry (Veeco/Sloan Dektak 3 ST, Plainview, New York, USA) on a given array of Si NMs after different times of immersion. The measurements were performed quickly (less than 30 min between extraction and re-immersion) to minimize formation of native oxide on silicon. Each reported data point corresponds to an average of at least 10 measurements; the error bars represent the standard deviations. Linear regression determined the dissolution rates. The rates correspond to the average of three experiments for each condition; the error bars represent the standard deviations.

DFT Simulations: Previous results demonstrate that DFT can accurately capture the atomic interactions between silicon structures and various molecules, as well as other materials under different conditions.^[28,30,33–36] Calculations reported here used the Spanish Initiative for Electronic Simulations with Thousands of Atoms (SIESTA) package.^[37] Parameterization of the exchange-correlation (XC) functional exploited both local density approximations (LDA) with CA,^[38] PW92,^[39] and generalized gradient approximations (GGA) with PBE,^[40] RPBE,^[41] PBEsol.^[42] The Si–K interaction was not computed using LDA, because the parameters in the pseudopotential for K are not yet available. Norm-conserving pseudopotentials described the core electrons.^[43] For the basis set generation, double zeta basis plus polarization (DZP) numerical atomic orbital was used. For Monkhorst-Pack k-point generation, $6 \times 6 \times 1$ was applied for structural relaxation.^[44] Vacuum regions with widths of ≈ 20 Å are introduced along the z-direction of the periodic box to prevent any unphysical effects near the boundaries. Structural relaxation corresponds to the condition when the maximum residual force of the system is less than 0.05 eV Å⁻¹. The maximum atomic displacements were initially 0.05 Å, but subsequently changed to 0.005 Å for final optimization when the maximum residual force was 0.1 eV Å⁻¹. A structure comprised of Si(100) with hydrogen (H) terminated surfaces approximated the experimental condition. The size of the simulation was 15.35×7.67 Å (total of 128 atoms).

MD Simulations: The chemical interactions of silicon with water and associated dissolution dynamics were captured by MD^[45] simulation with the Reaxff potential, integrated in the Large-scale Atomic/Molecular Massively Parallel Simulator (LAMMPS) package,^[46] for all atoms (silicon, oxygen, and hydrogen).^[47] The initial geometry included a Si NM with 120 silicon atoms, surface terminated with hydrogen and submersed in a box of water with 852 molecules. Periodic boundary conditions were used in all directions. Energy minimization of the system was performed for 1 000 000 steps. The time step was selected to be 0.1 fs, to ensure the capture of chemical reaction events between different atomic species.^[48] The Nosé–Hoover thermostat^[49] maintained the temperature at $T = 300$ K. The simulation was run for 95 ns and data were collected with the frequency of 1 ps.

Supporting Information

Supporting Information is available from the Wiley Online Library or from the author.

Acknowledgements

L.Y., A.B.F., and K.M. contributed equally to this work. Financial support from National Science Foundation (NSF, DMR 1242240, ECCS 1127480, and CBET 1264282). The experiments utilized the Frederick Seitz Materials Research Laboratory Central Facilities at the University of Illinois. The authors gratefully acknowledge the use of the parallel computing resource Blue Waters provided by the University of Illinois.

Received: October 3, 2014

Revised: January 3, 2015

Published online: January 27, 2015

- [1] S.-W. Hwang, H. Tao, D.-H. Kim, H. Cheng, J.-K. Song, E. Rill, M. A. Brenckle, B. Panilaitis, S. M. Won, Y.-S. Kim, Y. M. Song, K. J. Yu, A. Ameen, R. Li, Y. Su, M. Yang, D. L. Kaplan, M. R. Zakin, M. J. Slepian, Y. Huang, F. G. Omenetto, J. A. Rogers, *Science* **2012**, 337, 1640.
- [2] S.-W. Hwang, G. Park, H. Cheng, J.-K. Song, S.-K. Kang, L. Yin, J.-H. Kim, F. G. Omenetto, Y. Huang, K.-M. Lee, J. A. Rogers, *Adv. Mater.* **2014**, 26, 1992.
- [3] D. H. Kim, Y. S. Kim, J. Amsden, B. Panilaitis, D. L. Kaplan, F. G. Omenetto, M. R. Zakin, J. A. Rogers, *Appl. Phys. Lett.* **2009**, 95.
- [4] M. Irimia-Vladu, *Chem. Soc. Rev.* **2014**, 43, 588.
- [5] C. J. Bettinger, Z. Bao, *Adv. Mater.* **2010**, 22, 651.
- [6] M. Irimia-Vladu, P. A. Troshin, M. Reisinger, L. Shmygleva, Y. Kanbur, G. Schwabegger, M. Bodea, R. Schwödiauer, A. Mumyatov, J. W. Fergus, V. F. Razumov, H. Sitter, N. S. Saricifci, S. Bauer, *Adv. Funct. Mater.* **2010**, 20, 4069.
- [7] H. Tao, M. A. Brenckle, M. Yang, J. Zhang, M. Liu, S. M. Siebert, R. D. Averitt, M. S. Manno, M. C. McAlpine, J. A. Rogers, D. L. Kaplan, F. G. Omenetto, *Adv. Mater.* **2012**, 24, 1067.
- [8] L. Yin, H. Cheng, S. Mao, R. Haasch, Y. Liu, X. Xie, S.-W. Hwang, H. Jain, S.-K. Kang, Y. Su, R. Li, Y. Huang, J. A. Rogers, *Adv. Funct. Mater.* **2014**, 24, 645.
- [9] S.-K. Kang, S.-W. Hwang, H. Cheng, S. Yu, B. H. Kim, J.-H. Kim, Y. Huang, J. A. Rogers, *Adv. Funct. Mater.* **2014**, 24, 4427.
- [10] S.-W. Hwang, J.-K. Song, X. Huang, H. Cheng, S.-K. Kang, B. H. Kim, J.-H. Kim, S. Yu, Y. Huang, J. A. Rogers, *Adv. Mater.* **2014**, 26, 3905.
- [11] S.-W. Hwang, X. Huang, J.-H. Seo, J.-K. Song, S. Kim, S. Hage-Ali, H.-J. Chung, H. Tao, F. G. Omenetto, Z. Ma, J. A. Rogers, *Adv. Mater.* **2013**, 25, 3526.
- [12] L. Yin, X. Huang, H. Xu, Y. Zhang, J. Lam, J. Cheng, J. A. Rogers, *Adv. Mater.* **2014**, 26, 3879.
- [13] C. Dagdeviren, S.-W. Hwang, Y. Su, S. Kim, H. Cheng, O. Gur, R. Haney, F. G. Omenetto, Y. Huang, J. A. Rogers, *Small* **2013**, 9, 3398.
- [14] V. Lehmann, *Electrochemistry of Silicon: Instrumentation, Science, Materials and Applications*, Wiley-VCH, Weinheim, Germany **2002**.
- [15] W. Zhou, X. Dai, T.-M. Fu, C. Xie, J. Liu, C. M. Lieber, *Nano Lett.* **2014**, 14, 1614.
- [16] J. D. Birchall, J. S. Chappell, *Clin. Chem.* **1988**, 34, 265.
- [17] J. A. Raven, *Biol. Rev.* **1983**, 58, 179.
- [18] S.-W. Hwang, G. Park, C. Edwards, E. A. Corbin, S.-K. Kang, H. Cheng, J.-K. Song, J.-H. Kim, S. Yu, J. Ng, J. E. Lee, J. Kim, C. Yee, B. Bhaduri, Y. Su, F. G. Omenetto, Y. Huang, R. Bashir, L. Goddard, G. Popescu, K.-M. Lee, J. A. Rogers, *ACS Nano* **2014**, 8, 5843.
- [19] S. H. C. Anderson, H. Elliott, D. J. Wallis, L. T. Canham, J. J. Powell, *Phys. Status Solidi A* **2003**, 197, 331.
- [20] J.-H. Park, L. Gu, G. von Maltzahn, E. Ruoslahti, S. N. Bhatia, M. J. Sailor, *Nat. Mater.* **2009**, 8, 331.
- [21] H. Seidel, L. Csepregi, A. Heuberger, H. Baumgartel, *J. Electrochem. Soc.* **1990**, 137, 3612.
- [22] H. Seidel, L. Csepregi, A. Heuberger, H. Baumgartel, *J. Electrochem. Soc.* **1990**, 137, 3626.
- [23] D. Tie, F. Feyerabend, N. Hort, R. Willumeit, D. Hoeche, *Adv. Eng. Mater.* **2010**, 12, B699.
- [24] J. Walker, S. Shadanbaz, N. T. Kirkland, E. Stace, T. Woodfield, M. P. Staiger, G. J. Dias, *J. Biomed. Mater. Res., Part B* **2012**, 100B, 1134.
- [25] R. Leis-Sousa, M. J. Caldas, *Phys. Rev. B* **2011**, 84, 205314.
- [26] R. Konečný, D. J. Doren, *J. Chem. Phys.* **1997**, 106, 2426.
- [27] H. Q. Shi, M. W. Radny, P. V. Smith, *Surf. Sci.* **2004**, 561, 215.
- [28] J. Y. Lee, M.-H. Kang, *Phys. Rev. B* **2004**, 69, 113307.
- [29] J. A. Dean, N. A. Lange, *Lange's Handbook of Chemistry*, McGraw-Hill, New York **1992**.
- [30] H. Shi, M. Radny, P. Smith, *Surf. Sci.* **2004**, 561, 215.
- [31] P. M. Dove, D. A. Crerar, *Geochim. Cosmochim. Acta* **1990**, 54, 955.
- [32] H. A. Claessens, M. A. van Straten, J. J. Kirkland, *J. Chromatogr. A* **1996**, 728, 259.
- [33] R. Leis-Sousa, M. J. Caldas, *Phys. Rev. B* **2011**, 84, 205314.
- [34] W. Ye, K. Min, P. P. Martin, A. A. Rockett, N. Aluru, J. W. Lyding, *Surf. Sci.* **2012**, 609, 147.
- [35] B. Kumar, K. Min, M. Bashirzadeh, A. B. Farimani, M.-H. Bae, D. Estrada, Y. D. Kim, P. Yasaei, Y. D. Park, E. Pop, *Nano Lett.* **2013**, 13, 1962.
- [36] K. Min, A. B. Farimani, N. Aluru, *Appl. Phys. Lett.* **2013**, 103, 263112.
- [37] J. M. Soler, E. Artacho, J. D. Gale, A. García, J. Junquera, P. Ordejón, D. Sánchez-Portal, *J. Phys.: Condens. Matter* **2002**, 14, 2745.
- [38] J. P. Perdew, A. Zunger, *Phys. Rev. B* **1981**, 23, 5048.
- [39] J. P. Perdew, Y. Wang, *Phys. Rev. B* **1992**, 45, 13244.
- [40] J. P. Perdew, K. Burke, M. Ernzerhof, *Phys. Rev. Lett.* **1996**, 77, 3865.
- [41] B. Hammer, L. B. Hansen, J. K. Nørskov, *Phys. Rev. B* **1999**, 59, 7413.
- [42] J. P. Perdew, A. Ruzsinszky, G. I. Csonka, O. A. Vydrov, G. E. Scuseria, L. A. Constantin, X. Zhou, K. Burke, *Phys. Rev. Lett.* **2008**, 100, 136406.
- [43] N. Troullier, J. L. Martins, *Phys. Rev. B* **1991**, 43, 1993.
- [44] H. J. Monkhorst, J. D. Pack, *Phys. Rev. B* **1976**, 13, 5188.
- [45] A. C. T. van Duin, S. Dasgupta, F. Lorant, W. A. Goddard, *J. Phys. Chem. A* **2001**, 105, 9396.
- [46] S. Plimpton, *J. Comput. Phys.* **1995**, 117, 1.
- [47] J. C. Fogarty, H. M. Aktulga, A. Y. Grama, A. C. T. van Duin, S. A. Pandit, *J. Chem. Phys.* **2010**, 132.
- [48] A. C. T. van Duin, A. Strachan, S. Stewman, Q. S. Zhang, X. Xu, W. A. Goddard, *J. Phys. Chem. A* **2003**, 107, 3803.
- [49] D. J. Evans, B. L. Holian, *J. Chem. Phys.* **1985**, 83, 4069.